Operational Reliability Evaluation of Urban Multi-Energy Systems With Equivalent Energy Storage

Sheng Wang, *Member, IEEE*, Hongxun Hui, *Member, IEEE*, Yi Ding, *Member, IEEE*, Chengjin Ye, *Member, IEEE*, and Menglian Zheng, *Member, IEEE*

***Abstract*—With the coordination of multiple energies at the city level, the complexity of the urban energy system is ever-increasing. Securing the reliable operation of the urban multi-energy system (UMES) has become a challenging task. This article focuses on the operational reliability evaluation of the UMES considering the incorporation of equivalent energy storages. First, a novel concept of dynamic energy hub is proposed, as a unified tool to characterize the dynamic relationships of the operating conditions of diverse components in the UMES. Then, the temperature-controlled load (TCL) is modeled as the equivalent energy storage considering the thermal dynamics. Its operational reliabilities, as well as multiple other components, are modeled using the reliability equivalent technique to reduce the dimension of uncertainties. Moreover, a contingency management scheme of the UMES is developed in an optimal control framework considering the comfort costs of equivalent energy storages. To deal with the time-dependency of the optimal control problem, a simplified Benders decomposition procedure is devised and embedded in the Time-sequential Monte Carlo simulation to improve the computation efficiency of the reliability evaluation. Finally, a practical case of a UMES in southern China is used to validate the proposed technique.**

***Index Terms*—Dynamic energy hub, equivalent energy storage, operational reliability, simplified benders decomposition, urban multi-energy systems.**

Manuscript received 8 August 2022; revised 2 November 2022; accepted 29 November 2022. Date of publication 26 December 2022; date of current version 20 March 2023. Paper 2022-ESC-0862.R1, presented at the 2021 IEEE/IAS Industrial and Commercial Power System Asia (I&CPS Asia), Chengdu, China, Jul. 18–21, and approved for publication in the IEEE TRANSACTIONS ON INDUSTRY APPLICATIONS by the Energy Systems Committee of the IEEE Industry Applications Society. This work was supported in part by the Natural Science Foundation of Jiangsu Province, China, Operational reliability evaluation of multi-source and heterogeneous urban multi-energy systems, under Grant BK20220261, and in part by the Science and Technology Development Fund, Macau SAR, under Grants SKL-IOTSC(UM)-2021-2023 and 0003/2020/AKP. *(Corresponding authors: Hongxun Hui; Yi Ding.)*

Sheng Wang is with the State Key Laboratory of Internet of Things for Smart City, the Department of Electrical and Computer Engineering, University of Macau, Macao 999078, China, and also with the State Grid Suzhou City and Energy Research Institute Co. Ltd., Suzhou 215163, China (e-mail: wangsheng_zju@zju.edu.cn).

Hongxun Hui is with the State Key Laboratory of Internet of Things for Smart City and the Department of Electrical and Computer Engineering, University of Macau, Macao 999078, China (e-mail: hongxunhui@um.edu.mo).

Yi Ding and Chengjin Ye are with the College of Electrical Engineering, Zhejiang University, Hangzhou 310027, China (e-mail: yiding@zju.edu.cn; yechenjing@zju.edu.cn).

Menglian Zheng is with the College of Energy Engineering, Zhejiang University, Hangzhou 310027, China (e-mail: menglian_zheng@zju.edu.cn).

Color versions of one or more figures in this article are available at https://doi.org/10.1109/TIA.2022.3232099.

Digital Object Identifier 10.1109/TIA.2022.3232099

NOMENCLATURE

Indices

i	Index for node in Energy Hub.
j	Index for a specific component (e.g., a room cluster, a gas boiler, etc.).
s	Index for system state.
k	Index for time step.
l	Index for energy type.
v	Index for iteration time in Benders decomposition.

Sets, matrixes, and functions

$\mathbf{d}$	Set of multiple energy loads.
$\mathbf{H}$	Energy conversion matrix.
$\mathbf{g}$	Set of multiple energy supplies.
$\mathbf{x}$	Set of state variables.
$\mathbf{u}$	Set of control variables.
$\mathbf{y}$	Set of output variables.
$\boldsymbol{\alpha}, \boldsymbol{\beta}, \boldsymbol{\chi}, \boldsymbol{\delta}$	Sets of coefficient matrixes in the dynamic energy hub model.
Φ_j	Cycle life loss function.
PPD	Predicted Percentage of Dissatisfied function.
$flag$	Flag function.
$\mathbf{u}^{MP}$	Set of control variables in the mater problem.
$\mathbf{u}_k^{SP}$	Set of control variables in the subproblem in time step k.
$\boldsymbol{\kappa}$	Set of Farkas dual variable of the subproblem.
$\mathbf{A}_k^{MP}$	Coefficient matrix with respect to the master problem.
$\mathbf{A}_k^{SP}$	Coefficient matrix with respect to the subproblem.
$\mathbf{b}$	Right-hand-side matrix.
PMV	Predicted Mean Vote function.
S	Set of system state.
CDF^l	Customer damage function of energy type l.

Variables

$es_{i,j}$	Energy storage j at node i.
$f_{i,j}^{sd}$	Self-dissipation term for component j at node i.
T_j^r	Indoor temperature of room j.
f_i^e, f_i^g	Electricity flow and gas flow from node i to electricity and gas buses, respectively.
f_i^h, f_i^c	Heat flow and cooling flow from node i to heat and cooling buses, respectively.

$C^{dg}_{i,j,k}$ Degradation cost of component j at node i at time step k.
$\delta^0_{j,k}$ Cycle depth of electric energy storage j in time step k before charging or discharging.
$\Delta\delta_{j,k}$ Increase of cycle depth EES j at time step k.
$C^{op}_{i,j,k}$ Comfort cost of equivalent energy storage j at node i in time step k.
C, C^{ES} Total cost and external cost.
C^{DEH}_k Operating cost of the urban multi-energy systems in time step k.
γ Operating mode of electric heat pump.
$EDNS^l$ Expected demand not supplied of energy type l.
$LOLP^l$ Loss of load probability of energy type l.
lc^l_k Load curtailment of energy type l at time step k.
ψ Auxiliary variable for total cost in Benders decomposition.
ϕ_k Auxiliary variable for operating cost at time step k in Benders decomposition.
T Temperature.

Parameters

C^a, ρ^a Specific heat capacity and density of the air.
V_j space of the room j.
$T^{\max}_j$ Upper bound for the comfort zone of room j.
$T^{\min}_j$ Lower bound for the comfort zone of room j.
T^a Ambient temperature.
K_j Heat transfer coefficient for room j.
A^s_j Area of the room j exposed to outside.
N^{ex}_j Air exchange frequency of room j.
ε_j coefficient of heat released by appliances and occupants of room j.
A_j Living area of the room.
T^*_j Most comfortable temperature.
$f^{c,chr,\max}_{i,j}$ Maximum discharging power of equivalent energy storage j at node i.
$es^{\max,s}_i$ Energy storage capacity of node i in state s.
NJ Number of clusters of rooms.
NC_j Number of rooms in the cluster j.
NK Number of time steps.
NS Number of system states.
$\lambda^{TCL}_{s,s'}$ State transition rate of temperature-controlled load from state s to s'.
λ^{ICS}, μ^{ICS} Failure and repair rates of information and communication system.
λ^p, μ^p Failure and repair rates of prime mover subsystem.
λ^e, μ^e Failure and repair rates of electricity-generation subsystem.
λ^h, μ^h Failure and repair rates of heat-production subsystem.
(H_A, E_A) Extreme point A of the feasible region of the combined heat and power plant.
N^{GB} Number of gas boiler.
$C^{inv}_{i,j}$ Investment cost of component j at node i.
C^{inv}_i Investment cost of the component at node i.
T_i Lifecycle of energy storage at node i.
σ Constant coefficient of Predicted Percentage of Dissatisfied function.
ρ^g_k, ρ^e_k Nodal gas and electricity prices at time step k.
ξ Threshold of convergence.
τ System state duration.
UB, LB Upper and lower bounds of Benders iteration.

I. Introduction

CITY accounts for 60%–80% of the energy consumption in the world [1]. Toward a low-carbon energy future, multiple energies, including electricity, gas, heat, and cooling, are tightly coupled and interacted at the city level, named urban multi-energy systems (UMES). For example, as a typical facility that couples primary energies with electricity and heat, the combined heat and power plant (CHP) is being installed widely (e.g., CHP reaches 81.68 GW by the end of 2020 in the US) [2]. The UMES can take various forms and configurations, such as architectural complexes, industrial parks, etc., to promote overall energy utilization efficiency.

Despite the benefits, the interdependency among multiple energy systems also brings challenges to the reliable operation of UMES. For example, if the CHP fails, the operation of the downstream component that relies on the heat produced by the CHP, such as the absorption chiller (AB), may be affected. Many incidents are witnessed worldwide. In Dec 2020, in Lvliang, China, the coal handling belt of Datuhe CHP was frozen, which interrupted the heat supply of the 11×10^6 m^2 urban area for three days [3]. Therefore, the operational reliability evaluation of UMES is urgently required.

Some studies focus on the flexibility modeling of UMES, which can support the reliable operation in contingencies. Energy hub (EH) is an important concept proposed by [4], which can be used to characterize the energy conversion relationships among multiple energies at the city level. The quantitative exploration of EH flexibility in terms of the electricity-shifting curve is conducted in [5] based on aggregated utility curve of multi-energy demands. The day-ahead optimal dispatch is formulated for the UMES in [6] considering the power-to-gas facilities and dynamics pipeline networks. The incentive mechanism is designed in [7] to activate the flexibilities of residential EHs. The optimal operation of EHs is performed to mitigate network congestion in [8] with large-scale distributed energy resources. A holistic assessment framework is developed in [9] to use the operational flexibility of public transport hubs to harness the reliability and economic performance of the UMES. The flexibility of EH is used to enhance the resilience of the distribution system in [10], where a pre- and post-disaster management scheme is proposed.

Recently, some studies have been dedicated to assessing the reliability of UMES [11], [12], [13]. References [14], [15], [16] establish the reliability modeling methods for multi-performance and multi-state systems, which set a solid foundation for the reliability evaluation of UMES. The appliances on the customer side are modeled as flexible resources in [17] to improve the operational reliability of the EH. The concept of exergy is used in [18] to evaluate the reliability of the UMES

with different energy qualities. The impacts of different levels of demands and various weather situations on the reliability of UMES are investigated in [19]. A data-driven reliability evaluation method is proposed for UMES in [20] based on probabilistic deep learning and the Gaussian mixture model-hidden Markov model. Improved Shapley value is used in [21] to trace the reliability of UMES. A systematic framework for assessing the reliability of energy supply in integrated energy systems is developed in [22] based on a quasi-steady-state model. Resilience and reliability are both tackled in [23] in the optimization of UMES with thermal energy storage.

However, several key issues have not been well addressed in previous research. For example, the impact of flexible resources on the reliability of UMES has not been comprehensively investigated. As a typical flexible resource, temperature-controlled loads (TCLs) account for more than 40% of the total power consumption in the urban area, which can be utilized to promote the reliability of the UMES [24]. In the winter, when the energy supply to the TCL is interrupted (e.g., electricity to air conditions, hot water to the heat exchangers), the temperature of the room can still be maintained near the most comfortable values for a short period due to the thermal dynamics of rooms [25], [26]. Moreover, the heat can also be over-supplied, which is equivalent to increasing the energy stored in the rooms [27]. By this means, if the heat supply is interrupted, the indoor temperature can be maintained at a comfortable value for a longer period. Therefore, TCLs can be regarded as equivalent energy storage by charging and discharging strategies. They can be utilized to assist the reliable operation of the UMES.

The utilization of TCL in the optimal operation of electricity systems has been studied recently. The air conditions are modeled as the operating reserve in [26], and the capacity, ramping speed, etc., are quantitatively characterized. A forecasting method for the control capacity and control payback of aggregated TCL in the demand response is proposed in [28]. The regulation capacity of TCLs under hybrid cyber-attacks is evaluated in [29], and a distributed event-based control method is proposed. A robust and hierarchical control mechanism for aggregated TCL is proposed in [30] to deal with the uncertainties and computation burden issues. The TCLs are used for the frequency regulation in [31], and the impact of communication latency is investigated [32]. The coordinated control of distributed generators and TCLs for the restoration of the urban microgrid is proposed in [33]. Though the TCL can be utilized for the electricity system operation, the impacts of its equivalent energy storage on the operational reliability of UMES have rarely been investigated.

Introducing the equivalent energy storage of TCL can increase the complexity of the reliability evaluation of UMES. TCLs are usually large-scale and heterogeneous. The number of state spaces will grow exponentially with the increase of TCLs [34]. Thus, a unified physical and reliability modeling technique, as well as a state-space reduction technique, are required to reduce the dimension of control variables and uncertainties. Moreover, with the participation of various energy storages, the original optimal operation of the UMES becomes a time-dependent optimal control problem. The computation burden may grow significantly, especially in the reliability evaluation procedure in which the optimal control problem has to be solved many times. In previous studies, linearization techniques are usually adopted to simplify the model [35], [36]. However, this method is not applicable for reducing the dimension of uncertainty, or relaxing the time dependency.

To address the aforementioned issues, this paper proposes an operational reliability evaluation framework for UMES. The contributions are summarized as follows:

1) A novel concept of the dynamic energy hub (DEH) model is proposed. Compared with the traditional EH model, the proposed DEH model uses system state equations to characterize the dynamic relations of both energy conversion and energy storage components in a linear and unified manner.
2) A multi-state operational reliability model of large-scale heterogeneous TCLs is developed. The joint impacts of the information and communication system (ICS) failure and equivalent energy storage are characterized in this model. The reliability equivalent technique is proposed to reduce the dimension of the system state and the complexity of the subsequent optimal control problem.
3) A contingency management scheme (CMS) of the UMES is proposed. The degradation cost increment of physical energy storage due to the irregular charging/discharging, and the comfort cost of TCLs, are both quantified. By this means, the joint impacts of energy storage aging and TCL comfort zone on the reliability of UMES can be assessed.
4) A simplified Benders decomposition procedure is devised to improve the computation efficiency of the operational reliability evaluation. By decoupling the subproblems and relaxing some of the Benders procedures, the time dependency from energy storage in most scenarios can be relaxed. The computation complexity can be reduced.

II. Model of the UMES Using the Concept of DEH

The UMES is at the distribution level of the energy systems. Configured by various energy conversion devices, energy storage devices, etc., the UMES can flexibly consume the electricity and gas from energy transmission systems, and satisfy the electricity, heat, and cooling loads of end-users. A typical example of the configuration is presented in Fig. 1, including CHP, gas boiler (GB), electric heat pump (EHP), distributed generator (DG), electricity energy storage (EES), thermal energy storage (TES), and ice storage (IS). The end-users have electricity, heat, and cooling loads, whereas the last two types further consist of TCL (e.g., heat exchanger) and non-TCL (e.g., direct use of hot water). In this paper, the TCL can be regarded as equivalent energy storage, assisting in improving the reliability of UMES. The above components and loads are all abstracted as different nodes, as in Fig. 1. The concept of energy buses, including the electricity, gas, heat, and cooling buses serve as conjunctions to model the energy concentrations and distribution [37].

In traditional studies, the Energy Hub (EH) model is usually adopted to describe the steady-state energy conversion relationship across multiple energy sectors of the UMES [38], [39]. As

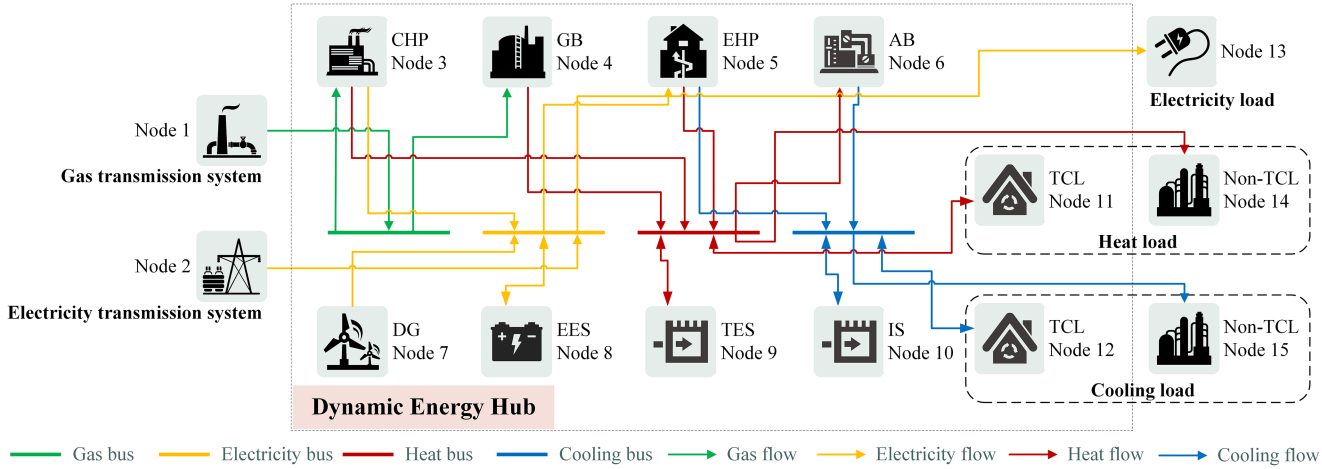

Fig. 1. Model of the UMES using the concept of dynamic energy hub.

in (1), $\mathbf{d}$, $\mathbf{H}$, and $\mathbf{g}$ represent the multi-energy loads, energy conversion matrix, and energy supply, respectively.

$$\mathbf{d} = \mathbf{H} \cdot \mathbf{g} \tag{1}$$

However, the participation of various energy storages and TCLs with different dynamic characteristics has transformed the traditional static system into a more complex and dynamic system. Thus, the traditional EH model becomes less competent in describing such characteristics of the UMES. Derived from the EH model, hereby we propose a Dynamic Energy Hub (DEH) model:

$$\begin{cases} d\mathbf{x}/dt = \boldsymbol{\alpha}\mathbf{x} + \boldsymbol{\beta}\mathbf{u} \\ \mathbf{y} = \boldsymbol{\chi}\mathbf{x} + \boldsymbol{\delta}\mathbf{u} \end{cases} \tag{2}$$

DEH model comprises a system state equation and output equation, where $\mathbf{x}$, $\mathbf{u}$, and $\mathbf{y}$ are the sets of state variables, control variables, and output variables, respectively. Symbols $\boldsymbol{\alpha}$, $\boldsymbol{\beta}$, $\boldsymbol{\chi}$, and $\boldsymbol{\delta}$ are corresponding coefficient matrixes. The specific elements in the coefficient matrixes depend on the physical system. In our UMES in Fig. 1, the specific elements can be found in Appendix A and [40]. Compared with the traditional EH model, the DEH can characterize the time-varying relations between chronological charging/discharging behaviors and the state of charge (SOC) of energy storages, the thermal dynamics of the room, the time-varying mass flow rate of the hot waters in the district heating pipelines, etc. Therefore, it can precisely reflect the dynamics of component conditions in UMES.

III. Operational Reliability Equivalent of Components in the UMES

A. Multi-State Operational Reliability Equivalent of TCL Considering the Thermal Dynamics

The equivalent energy storage of TCL originates from the thermal dynamics of the rooms. During the normal operating state, the indoor temperature is maintained to the desired comfortable value by the TCLs. When the contingency happens, the cooling energy supplied to the TCL may be interrupted for a short period (assuming the current season is summer). Then, the indoor temperature will increase, deviating from the desired comfortable value. Nonetheless, before the temperature reaches beyond the comfort zone, the cooling load for this user can be still regarded to be satisfied. During this process, the TCL can be regarded to have provided equivalent cooling energy to the UMES, as presented in Fig. 2. Besides, the cooling energy can also be over-supplied and the temperature may become lower than the desired comfortable value. This can be regarded as the cooling energy charging into the TCLs. In this case, if the contingency happens in the future, the pre-stored cooling energy can keep the temperature comfortable for a longer period. In summary, the TCL can both be charged and discharged, and therefore it can be equivalent to thermal or cooling storage.

The capacity of the equivalent energy storage of room j can be calculated as:

$$es_{12,j} = C^a \rho^a V_j \left(T_j^{\max} - T_j^{\min}\right) \tag{3}$$

where C^a and ρ^a are the specific heat capacity and density of the air, respectively; V_j is the space of the room; $T_j^{\max}$ and $T_j^{\min}$ are the upper and lower bounds for the comfort zone, respectively; $es_{12,j}$ is the equivalent energy storage capacity.

Different from other physical energy storages (EES, TES, and IS), the self-dissipation effect of the equivalent energy storage cannot be neglected during short-term operation. Self-dissipated energy $f_{12,j}^{sd}$ is also the cause of the increase in the indoor temperature, including the heat released by the appliances and occupants in the room, the heat transferred outside, and the heat leakage by air exchange [26]:

$$f_{12,j}^{sd}\left(T_j^r\right) = \left(T^a - T_j^r\right) K_j A_j^s + C^a \rho^a V_j^a \left(T^a - T_j^r\right) N_j^{ex} - \varepsilon_j A_j \tag{4}$$

where T_j^r is the indoor temperature; T^a is the ambient temperature; K_j is the heat transfer coefficient; A_j^s is the area of the room that is exposed to the outside; N_j^{ex} is the air exchange frequency; ε_j represents the coefficient of heat released by appliances and occupants; A_j is the living area of the room. Note that the self-dissipation term is related to the ambient temperature, and thus it is changing over time.

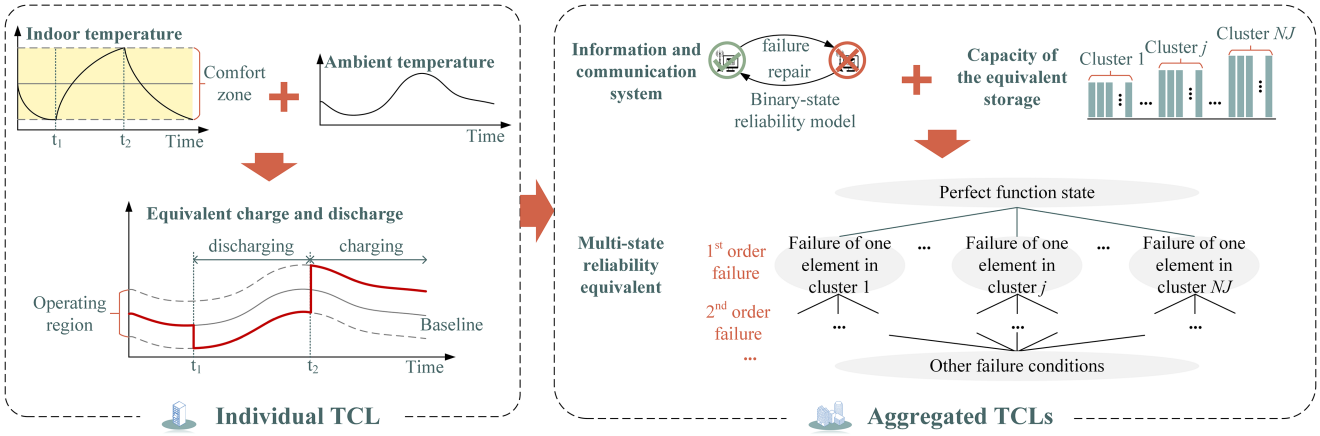

Fig. 2. Multi-state operational reliability equivalent of TCLs.

We assume that 1) the TCL always maintains the desired comfortable temperature T_j^* in normal conditions; 2) the temperature of the room is always maintained steadily, which means the cooling supplied to the room equals the self-dissipation value. Then, when the room temperature equals the most comfortable temperature, the self-dissipation value is regarded as the baseline for the TCL load. With the variation of ambient temperature, the baseline is also changing over time. Besides, we assume that during the charging and discharging of the equivalent energy storage, the temperature of the room should still be restrained within the comfort zone. Otherwise, it is regarded as load curtailment. Under these assumptions, the equivalent charging and discharging power can be calculated based on the difference between the actual cooling energy that is supplied to the TCLs and the baseline. Thus, the maximum discharging power of the equivalent energy storage $f_{12,j}^{c,chr,\max}$ is reached only when the indoor temperature reaches the upper bound of the comfort zone:

$$\begin{aligned} f_{12,j}^{c,chr,\max} &= f_{12,j}^{sd}\left(T_j^{\max}\right) - f_{12,j}^{sd}\left(T_j^*\right) \\ &= \left(T_j^{\max} - T_j^*\right) K_j A_j^s + C^a \rho^a V_j^a \left(T_j^{\max} - T_j^*\right) N_j^{ex} \end{aligned} \tag{5}$$

The maximum charging capability $f_{12,j}^{c,dis,\max}$ can be calculated when the indoor temperature is at the lower bound of the comfort zone:

$$f_{12,j}^{c,dis,\max} = \left(T_j^* - T^{\min}\right) K_j A_j^s + C^a \rho^a V_j^a \left(T_j^* - T^{\min}\right) N_j^{ex} \tag{6}$$

Note that although $f_{12,j}^{sd}(T_j^{\max})$ and $f_{12,j}^{sd}(T_j^*)$ are related to the ambient temperature, their difference $f_{12,j}^{c,chr,\max}$, as in (5) and (6), as well as the equivalent energy storage capacity in (3), are only related to the comfort zone and the characteristic of the rooms themselves. They are irrelevant to the ambient temperature. This characteristic provides the system operator with predictability in managing their equivalent energy storages.

The model above describes the physical characteristic of a single TCL. Generally, for a UMES with large-scale heterogeneous TCLs, reliability issues become unneglectable. The control of TCLs relies tightly on the ICS. Sometimes when the ICS of a specific TCL fails, it can no longer serve as the equivalent energy storage until it is fully repaired [41]. If we simultaneously consider all the possible states of TCLs, the number of the state space will grow exponentially. Therefore, to reduce the dimension of the state space and improve the computation efficiency, the reliability equivalent technique is adopted [42].

The reliability of each TCL is represented by a binary-state Markov model independently. The idea of reliability equivalent is to aggregate the states that have the same performance. For example, the performances (i.e., the maximum charging/ discharging power, and the equivalent storage capacity) of TCLs in the cluster j are identical, as presented in Fig. 2. Then, the failure of any one TCL in this cluster will lead to a same derated performance for this cluster. Therefore, the states where one TCL fails can be regarded as the same state. By this means, the reliability of multiple binary-state TCL can be represented by a single multi-state reliability equivalent, and the number of states in reliability evaluation can be significantly reduced. In this paper, the multi-state reliability equivalent of the aggregated TCLs considers up to 2nd order failure. For NJ cluster of TCLs, the number of states is $(2 + NJ + NJ^2)$, which is substantially reduced compared with the original number of states $2^{\wedge}\sum_{j=1}^{NJ} NC_j$ without the reliability equivalent technique. NC_j is the number of rooms in the cluster j.

The state transition rate of aggregated TCLs between the perfect functioning state ($s = 1$) and the 1st order failure state ($s = j + 1$, if anyone TCL's ICS in the cluster j fails) can be calculated by:

$$\lambda_{1,j+1}^{TCL} = NC_j \lambda^{ICS},\ \lambda_{j+1,1}^{TCL} = \mu^{ICS} \tag{7}$$

where $\lambda_{1,j+1}^{TCL}$ is the state transition rate of aggregated TCLs from $s = 1$ to $s = j + 1$; $\lambda_{j+1,1}^{TCL}$ is the state transition rate of aggregated TCLs from $s = j + 1$ to $s = 1$; λ^{ICS} and μ^{ICS} are the failure and repair rates of the ICS, respectively.

The equivalent energy storage capacity and maximum charging power in state $s = j + 1$ can be calculated as:

$$es_{12}^{\max,s} = \sum_{j'=1}^{NJ} NC_{j'} es_{12,j'} - es_{12,j} \tag{8}$$

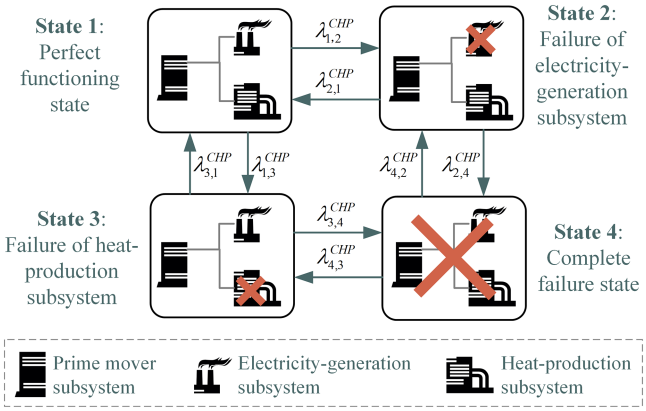

Fig. 3. Multi-state operational reliability model of CHP.

$$f_{12}^{c,chr,\max,s} = \sum_{j'=1}^{NJ} NC_{j'} f_{12,j'}^{c,chr,\max} - f_{12,j}^{c,chr,\max} \tag{9}$$

where $es_{12}^{\max,s}$ and $f_{12}^{c,chr,\max,s}$ are the capacity and maximum charging power of the equivalent energy storage in state s, respectively; $es_{12,j}$ and $es_{12,j'}$ represent the equivalent energy storage capacity of one single TCL in clusters j and j'.

The maximum discharging power $f_{12}^{c,dis,\max,s}$ can be calculated similarly. The state transition rates between the 1st order failure state and 2nd order failure state, as well as the equivalent energy storage capacity, the maximum charging and discharging power in the 2nd states can also be calculated similarly.

B. Operational Reliability Equivalent of Other Components

1) Multi-State Operational Reliability Model of CHP: Compared with TCLs, CHP is usually individually distributed. Therefore, here we emphasize the multi-state operational reliability model of a single CHP.

The CHP is a complex engineering system that is composed of three subsystems, namely, the prime mover system, the electricity-generation system, and the heat-production system [43]. The topology structure of the three subsystems is presented in Fig. 3. The reliability of each subsystem can be represented by a binary-state model. With the failure of different subsystems, the CHP presents four states. The state transition rate among the four states can be calculated as [40]:

$$\lambda_{1,2}^{CHP} = \lambda^e, \lambda_{2,1}^{CHP} = \mu^e, \lambda_{1,3}^{CHP} = \lambda^h, \lambda_{3,1}^{CHP} = \mu^h \tag{10}$$

$$\lambda_{2,4}^{CHP} = \lambda^h + \lambda^p, \lambda_{3,4}^{CHP} = \lambda^e + \lambda^p \tag{11}$$

$$\lambda_{4,2}^{CHP} = \frac{\mu^p\lambda^h\mu^h + \lambda^p\mu^h\mu^p}{\mu^p\lambda^h + \lambda^p\mu^h}, \lambda_{4,3}^{CHP} = \frac{\mu^p\lambda^e\mu^e + \lambda^p\mu^e\mu^p}{\mu^p\lambda^e + \lambda^p\mu^e} \tag{12}$$

where $\lambda_{1,2}^{CHP}$ represents the state transition rate between states 1 and 2; λ^e, λ^h, λ^p and μ^e, μ^h, μ^p are the failure and repair rates of electricity-generation, heat-production, and primary systems, respectively.

In the perfect functioning state, the feasible region of the CHP operation is a quadrangle defined by four extreme points (H_A, E_A), (H_B, E_B), (H_C, E_C), (H_D, E_D), which are four combinations of heat production and electricity generation [44]. If any subsystem fails, the feasible operating region is derated into the projection of the original feasible region on the corresponding axis. Therefore, the new feasible region can be expressed as:

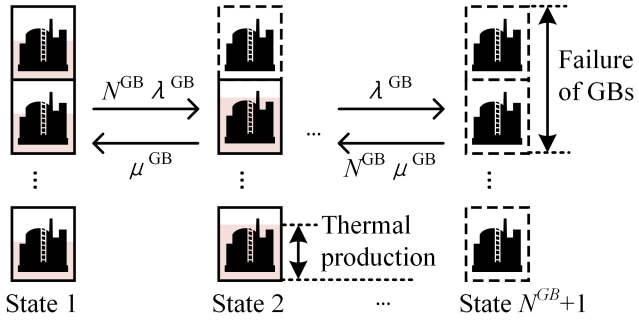

Fig. 4. Multi-state operational reliability equivalent of GBs.

$$f_3^e = 0 \tag{13}$$

$$f_3^h = 0 \tag{14}$$

$$\min\{H_A, H_B, H_C, H_D\} \le f_3^h \le \max\{H_A, H_B, H_C, H_D\} \tag{15}$$

$$\min\{E_A, E_B, E_C, E_D\} \le f_3^e \le \max\{E_A, E_B, E_C, E_D\} \tag{16}$$

where state 2 is subjected to (13) and (15); state 3 is subjected to (14) and (16); state 4 is subjected to (13) and (14).

2) Multi-State Operational Reliability Equivalent of Other Binary-State Components: For other components (i.e., GB, EHP, AB, DG, EES, TES, and IS in Fig. 1), they are usually configured in parallel with identical physical parameters. Take GB as an example. generally N^{GB} are configured in parallel in the UMES. The state-space diagram is presented in Fig. 4. The operational reliability of each GB is represented by a binary-state model. The operational reliability of a GB equivalent can be represented by a multi-state model. When some of the GB fails, the entire GB equivalent will not fail completely. Instead, it will be transferred into a derated state. Assuming the states of GB equivalent are sorted in a descendant order according to the available thermal production capacity. Then, the maximum heat production capacity in state s can be calculated as:

$$f_4^{h,s,\max} = \left(N^{GB} + 1 - s\right) f_4^{h,ind} \tag{17}$$

where $f_4^{h,ind}$ is the heat production capacity of a single GB in the perfect functioning state.

In the Markov process, it is assumed that only one state transition could happen at a time. Thus, the state transition could only happen between two adjacent states. The state transition rate between any two adjacent states, $\lambda_{s,s+1}^{GBs}$ and $\lambda_{s+1,s}^{GBs}$, can be calculated as:

$$\lambda_{s,s+1}^{GBs} = \left(N^{GB} + 1 - s\right)\lambda^{GB}, \lambda_{s+1,s}^{GBs} = s\mu^{GB} \tag{18}$$

where λ^{GB} and μ^{GB} are the failure and repair rates of a single GB, respectively. The operational reliability equivalents of other components can be determined with a similar approach.

IV. Contingency Management Scheme of the UMES Considering Various Cost of Energy Storages

Based on the multi-state operational reliability equivalents developed in Section III, the state sequence of the components over the operating horizon can be simulated using the time-sequential Monte Carlo simulation (TSMCS) technique. The detailed procedures are elaborated in Section V. During each simulation, if the electricity or gas supply is interrupted, or any component fails, the UMES may be re-dispatched. In an even worse case, some loads may be curtailed. Hence, in this section, a contingency management scheme (CMS) for the UMES is developed to minimize the load curtailment based on the optimal control framework by fully utilizing the flexibilities of energy conversion, energy storage devices, as well as the equivalent storage from the TCLs.

A. Degradation and Comfort Costs of Different Energy Storages

For the optimization of the CMS, it is important to measure the external cost during the operation. Besides the explicit cost of the consumed energies, another major part of the cost is from energy storages. The cost of physical energy storages (i.e., EES, TES, and IS) is mainly owing to degradation. For the equivalent energy storage from TCLs, the cost is mainly caused by the comfort loss due to the deviation from the desired comfortable temperature.

The EES in the UMES is usually configured by the lithium-ion battery. Its lifetime is short, and thus the degradation cost is unneglectable. In the CMS, the charging and discharging of the EES will become more frequent and irregular, which further accelerates the degradation process. Among various factors that affect the degradation, circle depth is the most unneglectable one and is tightly related to the CMS strategy.

The degradation cost of a single charging/discharging process related to the cycle depth in a time step can be calculated by [45]:

$$C^{dg}_{8,j,k} = C^{inv}_{8,j} \int_{\delta^0_{j,k}}^{\delta^0_{j,k}+\Delta\delta_{j,k}} \Phi_j(\delta) d\delta \tag{19}$$

where $C^{dg}_{8,j,k}$ is the degradation cost of the EES j at time step k; $C^{inv}_{8,j}$ is the placement cost of the EES j; $\delta^0_{j,k}$ is the cycle depth of EES j in time step k before charging or discharging; $\Delta\delta_{j,k}$ is the increase of cycle depth of EES j at time step k; Φ_j is the cycle life loss, which is elaborated in Appendix B.

The degradations of the TES and IS are calculated as the average depreciable cost:

$$C^{op}_9 = C^{inv}_9 / T_9 NK\Delta t, C^{op}_{10} = C^{inv}_{10} / T_{10} NK\Delta t \tag{20}$$

where C^{op}_9 and C^{op}_{10} are the depreciable costs of TES and IS respectively; C^{inv}_9 and C^{inv}_{10} are the investment costs of the TES and IS, respectively; T_9 and T_{10} are the lifecycles of the TES and IS, respectively; NK is the number of time steps.

The comfort cost of equivalent energy storage in summer $C^{op}_{12,j,k}$ can be evaluated using the Predicted Percentage of Dissatisfied (PPD) model [46]:

$$C^{op}_{12,j,k} = \sigma PPD_j \left(\left| T^*_{j,k} - es_{12,j,k} / \left(C^a \rho^a V_j \right) \right| \right) \tag{21}$$

where σ is the constant coefficient that transforms the PPD into the discomfort cost. The PPD function in its original form is a complex exponential function, which is difficult to be addressed by the solvers. Therefore, it is approximated into a quadratic function. The specific form is introduced in Appendix C [47].

The comfort cost in winter $C^{op}_{11,j,k}$ can also be calculated similarly. Therefore, the total operating cost from the energy storage C^{ES} can be calculated as:

$$C^{ES} = \sum_{k=1}^{NK} \sum_{j=1}^{NJ} \left(C^{dg}_{8,j,k} + \gamma C^{op}_{11,j,k} + (1-\gamma) C^{op}_{12,j,k} \right) + C^{op}_9 + C^{op}_{10} \tag{22}$$

where γ is a binary variable; $\gamma = 1$ and 0 represent winter and summer, respectively. It is assumed that in summer, EHP only operates in cooling mode, and the TCL only has cooling storage. Vice versa for winter.

B. CMS of UMES Based on Optimal Control Framework

The objective of the CMS of the UMES is to minimize the external cost C, including the energy purchasing cost, load curtailment cost, and the degradation and comfort costs of energy storages, as in (23). The control variable is $\mathbf{u}$, as described in Section II.

$$\underset{\mathbf{u}}{Min}\ C = C^{ES} + \sum_{k=1}^{NK} C^{DEH}_k \tag{23}$$

$$C^{DEH}_k = \rho^g_k f^g_{1,k} + \rho^e_k f^e_{2,k} + \sum_{l \in \{el,ht,cl\}} CDF^l lc^l_k \tag{24}$$

where C^{DEH}_k is the operating cost of UMES in time step k; ρ^g_k and ρ^e_k are the prices of gas and electricity, respectively; l represents the type of energy, where el, ht, and cl represent electricity, heat, and cooling, respectively. The optimal control framework is subjected to:

1) The system state and output equations of the DEH in (2).
2) The operating constraints for EES, TES, IS, and equivalent energy storages:

$$\begin{aligned} \mathbf{0} &\le [es_8, es_9, es_{10}, es_{11}, es_{12}] \\ &\le [es_8^{\max,s}, es_9^{\max,s}, es_{10}^{\max,s}, es_{11}^{\max,s}, es_{12}^{\max,s}] \\ &\quad \left[\left| f^e_8 \right|, \left| f^h_9 \right|, \left| f^c_{10} \right|, \left| f^h_{11} \right|, \left| f^c_{12} \right| \right] \end{aligned} \tag{25}$$

$$\le \left[f_8^{e,\max,s}, f_9^{h,\max,s}, f_{10}^{c,\max,s}, \gamma f_{11}^{h,\max,s}, (1-\gamma) f_{12}^{c,\max,s} \right] \tag{26}$$

3) The operating constraints for CHP in (13)–(16) according to different states. The operating constraint of GB in (17). The energy consumption constraints of the electricity and gas transmission system, and the operating constraints of

other devices (i.e., EHP, AB, and DG):

$$\mathbf{0} \le [f_1^g, f_2^e] \le [f_1^{g,\max,s}, f_2^{e,\max,s}] \tag{27}$$

$$\mathbf{0} \le \left[f_5^h, f_5^c\right] \le \left(N^{EHP} + 1 - s^{EHP}\right) \times \left[\gamma f_5^{h,ind}, (1-\gamma) f_5^{c,ind}\right] \tag{28}$$

$$\mathbf{0} \le [f_6^c, f_7^e] \le \left[\left(N^{AB} + 1 - s^{AB}\right) f_6^{h,ind}, f_7^{e,\max,s}\right] \tag{29}$$

4) Initial and terminal conditions of the energy storages. The amount of energy stored in the energy storage devices at the end of the studied period should be recovered to the values at the beginning of the studied period:

$$[es_{8,NK}, es_{9,NK}, es_{10,NK}, es_{11,NK}, es_{12,NK}] = [es_{8,1}, es_{9,1}, es_{10,1}, es_{11,1}, es_{12,1}] \tag{30}$$

5) Constraints for the load curtailment:

$$\mathbf{0} \le \left[-f_{13}^e, -f_{14}^h, -f_{15}^c\right] \le \left[f_{13}^{e,\max}, f_{14}^{h,\max}, f_{15}^{c,\max}\right] \tag{31}$$

6) The trivial constraints for energy flows:

$$\left[f_3^g, f_4^g, f_5^e, f_6^h\right] \le \mathbf{0}, f_7^e \ge 0 \tag{32}$$

where $es_i^{\max,s}$ represents the capacity of energy storage i in state s; $f_8^{e,\max,s}$ is the maximum charging/discharging power of EES in state s; N^{EHP} and N^{AB} are the numbers of EHP and AB, respectively; s^{EHP} and s^{AB} are the states of EHP and AB, respectively; $f_5^{h,ind}$ and $f_5^{c,ind}$ are the heat and cooling productions of a single EHP, respectively; $f_7^{e,\max,s}$ is the electricity generation capacity of DG in state s, which further depends on the type of the DG; $es_{8,NK}$ and $es_{8,1}$ represent the energy storage of EES when $k = NK$ and $k = 1$, respectively.

V. Operational Reliability Evaluation Procedure Using Simplified Benders Decomposition

A. Operational Reliability Indices

The expected demand not supplied (EDNS) and loss of load probability (LOLP) are usually adopted to evaluate the reliability of the electricity system. These two indices can be extended as follows to evaluate the operational reliability for multiple energies:

$$\begin{cases} EDNS^l(k) = \sum_{i=1}^{NS} lc_k^l / NS \\ LOLP^l(k) = \sum_{i=1}^{NS} flag(lc_k^l) / NS \end{cases} \tag{33}$$

where NS is the number of simulation times in the TSMCS; $flag(x)$ represents the flag function, where $flag(x) = 1$ when $x > 0$; otherwise $flag(x) = 0$.

The criterion for the convergence of TSMCS is given by the standard deviation of EDNS:

$$\sqrt{Var\left(EDNS^l(k)\right)} / EDNS^l(k) \le \xi \tag{34}$$

B. Operational Reliability Assessment Procedure

The above CMS is a large-scale, time-dependent quadric programming problem after approximating the polynomial terms in the objective function using Taylor expansion. It will be repeatedly solved many times in the TSMCS, which increases the computation burden dramatically. By observing the structure of the optimal control problem, we find that the state equation of the energy storage is the cause of the time interdependency. By fixing the state of the energy storage, the problem will become time-independent. Therefore, we divided the original problem into two problems: the state determination of the energy storage as the master problem, and the state determination of energy conversion devices as the subproblem.

Moreover, in the reliability evaluation procedure, the main purpose of the CMS is to avoid or minimize load curtailment, while the accurate solution for the operating cost is not mandatory. With these ideas in mind, here we devise a simplified Benders decomposition, and further, optimize the TSMCS procedure to improve the computation efficiency. The specific procedure is elaborated as follows:

Step 1: Initialization. Get the data and set the parameters.

Step 2: For each TSMCS, determine the initial state of the devices in the UMES, according to their steady-state probabilities [48]. It is assumed that the initial temperature is at the desired comfortable value for TCLs.

Step 3: Simulate the state sequence of components. Generate the random number U that follows the uniform distribution on $(0, 1)$. Assuming that the current state is s for the component. Then, the duration of the component being in this state τ can be calculated as:

$$\tau = \min\left\{-\lambda_{s,s'} / \ln(U_{s'}), s' \in S, s \ne s'\right\} \tag{35}$$

where S is the set of system states for this component. Then, the next state will be s'.

Step 4: Repeat Step 3 until the whole studied operating period is reached. Repeat Step 2∼Step 4 for all the components. generate the system state sequence by merging the component state sequences.

Step 5: For each TSMCS, solve the CMS problem. Set the upper and lower bounds for the Benders procedure: $UB^{(0)} = +\infty$, $LB^{(0)} = 0$, and the tolerance ζ.

Step 6: Solve the master problem:

$$\underset{\mathbf{u}^{MP}}{Min}\, \psi = C^{ES} + \sum_{k=1}^{NK} \phi_k \tag{36}$$

which is subjected to the state equations in (2), the related constraints (25), (26), (30), and the Benders cut from the sub-problem; $\mathbf{u}^{MP} = [f_{8,k}, f_{9,k}, f_{10,k}, f_{11,k}, f_{12,k}], k = 1, \ldots, NK$ is the control variable for the master problem. The cost from the subproblem ϕ_k is initialized as $\phi_k \ge 0$. Denote the solution of the master problem in the v_{th} iteration as $\mathbf{u}_{(v)}^{MP}$, and the value of the objective function $\psi_{(v)}$. Update the lower bound $LB_{(v)} = \max\{LB_{(v-1)}, \psi_{(v)}\}$. Obtain the solution of $\mathbf{u}^{MP}$as $\mathbf{u}_{(v)}^{MP}$.

Step 7: Solve the subproblem. The following subproblem is formulated for each time step k, with $\mathbf{u}_{(v)}^{MP}$ from the above master problem:

$$\underset{\mathbf{u}_k^{SP}}{Min}\, \psi_k^{SP} = C_k^{DEH} \tag{37}$$

which is subjected to the output equation from (2), related constraints (27)–(29), (31), and (32). Here the control variable is $\mathbf{u}_k^{SP} = [f_{3,k}^g, f_{4,k}^g, f_{5,k}^e, f_{7,k}^e, f_{13,k}^e, f_{6,k}^h, f_{14,k}^h, f_{15,k}^c]$. If this subproblem is infeasible, go to Step 8; otherwise, go to Step 9.

Step 8: Supplement the feasibility cut to the master problem:

$$\boldsymbol{\kappa}\left[\mathbf{A}_k^{MP}\right]^T \mathbf{u}_k^{MP} \le \boldsymbol{\kappa}\mathbf{b} \tag{38}$$

where $\boldsymbol{\kappa}$ is the Farkas dual variable of the subproblem; $\mathbf{A}_k^{MP}$and $\mathbf{b}$ are the coefficients when the constraints of the subproblem are written in a compact form:

$$\left[\mathbf{A}_k^{SP}, \mathbf{A}_k^{MP}\right]^T \left[\mathbf{u}_k^{SP}, \mathbf{u}_k^{MP}\right] \le \mathbf{b} \tag{39}$$

Step 9: Check if there is any load curtailment. If not, stop the Benders iteration, even if the optimal solution may not be reached. Otherwise, supplement the following optimality cut to the master problem:

$$\psi_k^{SP} \ge \boldsymbol{\kappa}\,\mathbf{b} - \boldsymbol{\kappa}\left[\mathbf{A}_k^{MP}\right]^T \left[\mathbf{u}_k^{MP}\right]^T \tag{40}$$

Step 10: Check if all the time steps have been iterated. If so, update the upper bound as in (41). Solve the new master problem with all Benders cuts as in Step 1. Otherwise, repeat from Step 3 for the next time step $k = k + 1$.

$$UB_{(v)} = \min\left\{UB_{(v-1)}, C_{(v)}^{ES} + \sum_{k=1}^{NK} \hat{\psi}_{(v)}^{SP}\right\} \tag{41}$$

Step 11: Check if the convergence criterion has been satisfied. If so, output the results. Otherwise, repeat the next Benders iteration from Step 5.

$$\left(UB_{(v)} - LB_{(v)}\right)/\left(UB_{(v)} + LB_{(v)}\right) < \zeta \tag{42}$$

Step 12: Calculate the operational reliability indices in (33) according to the load curtailments obtained from the Benders iterations. Check (34) for convergence. If converges, the final results of operational reliability indices are obtained. Otherwise, repeat the next TSMCS from Step 2.

VI. Case Studies

A test UMES derived from a practical science park in Hangzhou, China, is used in this section to validate the effectiveness of the proposed operational reliability evaluation technique. The structure of the UMES is the same as presented in Fig. 1. The electricity, heat, and cooling load profiles on a typical summer day are presented in Fig. 5. The electricity price is set according to the regulation of the National Development and Reform Commission using the Time-of-Use tariff. The gas price is set according to the contract price between the science park and the gas company.

The number and parameters of the components are listed in Table I. The failure and repair rates of the primal mover system

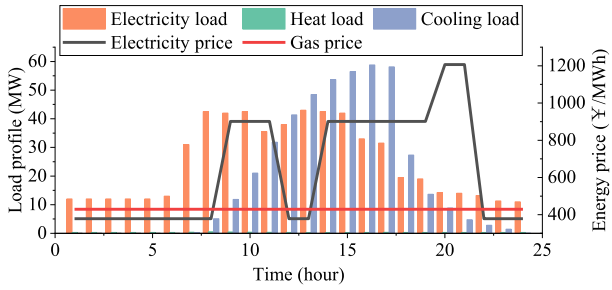

Fig. 5. Load profiles and energy prices.

TABLE I
Parameters of Components in the UMES

	Number	Properties
CHP	1	Extreme points: (0,25), (11,21), (9,0), (0,0) MW
GB	4	Heat capacity: 2.8 MW
EHP	3	Heat capacity: 6.4 MW; cooling capacity: 5.6 MW
AB	6	Cooling capacity: 6.33 MW
DG	1	Wind generator capacity: 4 MW
EES	6	Capacity: 2 MWh; maximum charging and discharging power: 1 MW; investment cost: 1.437×10^6 ¥/MW
TES	4	Capacity: 2 MWh; maximum charging/discharging power: 1 MW; investment cost: 1.01×10^5 ¥/MW
IS	8	Capacity: 17.58 MWh; maximum charging and discharging power: 8.79 MW; investment cost: 2.16×10^5 ¥/MW

are 1/2880 h^{-1} and 3/40 h^{-1}, respectively [49]. The failure and repair rates of the electricity-generation system, heat-production system, and other components are set to 1/960 h^{-1} and 1/40 h^{-1}, respectively [43], [50], [51]. The electricity generation and heat production efficiencies of CHP are 0.3 and 0.4, respectively [52]. The efficiencies of GB and AB are 0.8 and 0.7, respectively. The coefficients of performance of EHP in summer and winter are 4 and 3, respectively [53].

The science park has an 8×10^5 m^2 heating/cooling area. According to the types of buildings, the rooms are approximately aggregated into 200 clusters. Each cluster consists of 40 rooms with floor areas of [60, 200] m^2. The heat transfer coefficient is 7.69 w/(m^2·K). The wall area of each room is calculated based on its room area [26]. The air exchange frequency is set to 0.5 times/hour. The heat released by appliances or occupants is set to 4.3 w/m^2. The failure and repair rates of the ICS are set according to [41]. The comfortable temperature in summer is set to 26 °C. The upper and lower bounds for comfort zone are 28 °C and 24 °C, respectively.

A. Validation of the Computation Efficiency

The effectiveness of the proposed reliability evaluation technique for UMES is validated in this Section. The optimization model is formulated by the Yalmip modeling toolbox on MATLAB, and is solved by using the Mosek solver [54]. The numerical simulation is performed on a desktop with Intel(R) Core(TM) i7-10700 CPU and 16 GB RAM.

The convergences of the reliability indices are presented in Fig. 6. It can be observed that with about 10000 times Monte Carlo simulations, the reliability indices of electricity $EDNS^{el}$

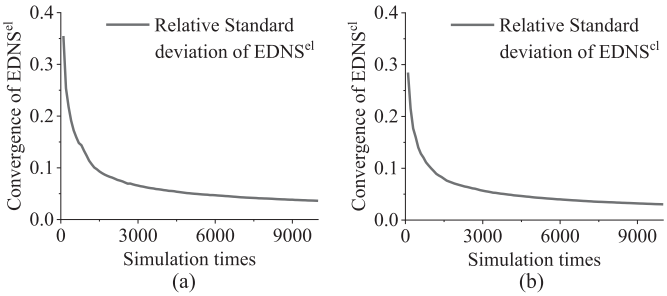

Fig. 6. Convergence curve of the TSMCS.

TABLE II
COMPARISONS OF COMPUTATION TIMES WITH/WITHOUT PROPOSED TECHNIQUES

Reliability equivalent technique	Simplified Benders decomposition	Computation time (s)
/	/	1904
√	/	881
√	√	116

and the cooling loads $EDNS^{cl}$ have both converged within a reasonable range. Furthermore, the computation times with different techniques are compared in Table II. It can be seen that with the utilization of the reliability equivalent technique, the computation time can be substantially reduced by 53.73%. By further introducing the simplified Benders decomposition, the over-calculation in most of the simulations can be avoided, and the computation time is further reduced by 86.83%.

B. Operating Condition of UMES in Representative Scenarios

To validate the effectiveness of the proposed CMS in managing the contingency states, the operating condition of UMES in four scenarios (i.e., S1, S2, S3, and S4) are compared. S1 is the normal operating state. In S2, the CHP fails completely. In S3, a set of EHP fails. In S4, two ISs fail.

The operating condition of the UMES in S1 is presented in Fig. 7 as the base scenario. Positive values represent the electricity, gas, heat, and cooling energy supplied by the energy transmission systems, and energy production and discharging from components. Negative values represent the energy consumption of devices and loads, and the charging to the energy storage. It can be observed from Fig. 7(a) that the electricity load is mainly supplied by the electricity transmission system. However, with the increase in electricity price at 9:00 in Fig. 5, the gas consumption begins to increase, as shown in Fig. 7(b). The CHP begins to consume gas to generate electricity and heat for providing cooling energy, instead of using the EHP. During the flat price of electricity at noon in Fig. 5, because electricity becomes more cost-efficient than gas again, the supply of gas drops during 12:00∼13:00 in Fig. 7(b). Moreover, it can be observed in Fig. 7(c) that the ISs play an important role in balancing the cooling load among different time periods. During the night hours, the EHP is working at a lower cost to charge cooling energy to ISs. During the day, the ISs operate in discharging mode to reduce energy cost. In addition, the variation of temperature of TCL can be limited to 0.075 °C in S1.

TABLE III
OPERATING CONDITIONS AND COST IN REPRESENTATIVE SCENARIOS

	S1	S2	S3	S4
Heat produced by GBs (MWh)	80.36	111.77	105.70	86.43
Cooling produced by ABs (MWh)	112.66	72.57	156.52	132.15
Heat exchanged by TESs (MWh)	23.74	16.00	21.10	23.74
Cooling exchanged by ISs (MWh)	287.46	286.29	281.34	192.96
Variation of TCL temperature	0.49%	100%	100%	100%
Cooling load curtailment (MWh)	0	30.16	20.69	26.66
Energy purchasing cost (¥)	4.81×10^5	4.71×10^5	5.06×10^5	4.94×10^5
Load curtailment cost (¥)	0	6.82×10^5	4.68×10^5	6.02×10^5
Degradation cost of energy storages (¥)	7.05×10^3	7.12×10^3	7.59×10^3	7.52×10^3
Comfort cost of TCLs (¥)	36.66	2.24×10^4	2.24×10^4	2.68×10^4

The detailed energy balancing in a partial failure scenario S3 is presented in Fig. 8. As shown in Fig. 8(a), the electricity consumption is reduced by 9.09% due to the EHP failure. The electricity balance is still maintained. As shown in Fig. 8(c), the CHP needs to ramp up during the electricity price valley hours (12:00-13:00) to cover the cooling supply shortage of EHP. Therefore, the gas consumption in this period increases, as shown in Fig. 8(b). As a result, more cooling energy needs to be provided by AB instead of EHP, as shown in Fig. 8(d). Nevertheless, the cooling load is still curtailed for 20.69 MWh.

The comparisons between the base scenario S1 and other scenarios are presented in Table III. It can be seen that the failure of components does impact the operating condition of the UMES substantially. In S2, the heat production shortage due to the failure of CHP is covered in part by GB, while some of the heat production is still uncovered. Therefore, the AB cannot work to its full potential, which leads to the curtailment of the cooling load. In S3, the EHP fails by a substantial amount. The shortage of cooling production is partly covered by AB, which is less economical and results in a higher energy purchasing cost. Besides, this failure mode further increases the irregular charging and discharging of energy storage, which leads to a higher degradation cost. In S4, with the failure of ISs, although the total energy production capability of the system has not been affected, the capability of balancing the energy among different time periods deteriorates. It also causes load curtailment. Throughout S2 to S4, we find that in all scenarios, the TCL is active in regulating the energy balance within the comfortable temperature zone.

To demonstrate the energy balance of the UMES with more severe failure, scenario S5 is set. In S5, all ABs fail. As shown in Fig. 9(d), because we can no longer rely on ABs to provide the cooling energy, the cooling supplies from EHPs and ISs increase slightly to their upper limits. The cooling load is still curtailed for 101.07 MWh. Moreover, the heating energy that is used to satisfy the ABs is no longer needed, and therefore, the gas and

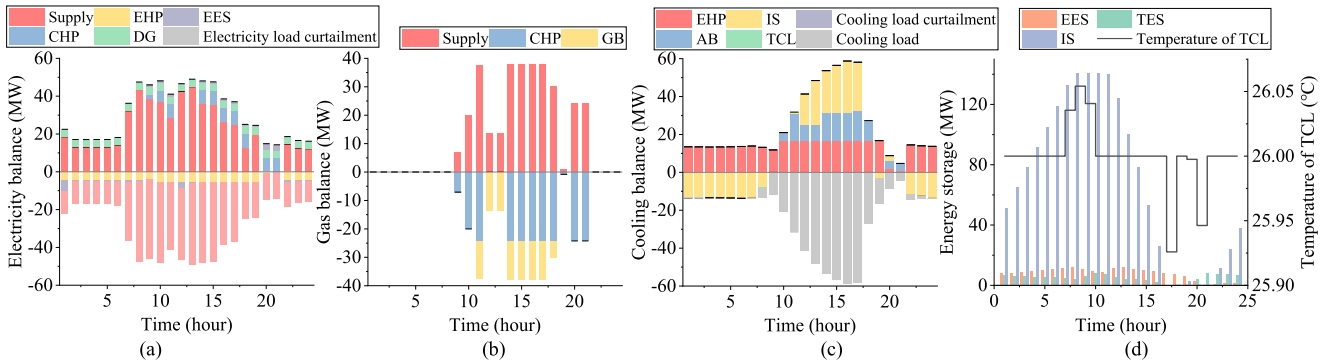

Fig. 7. Operating conditions of the UMES components in S1: (a) Electricity balance; (b) Gas balance; (c) Cooling balance; (d) Energy storage and TCL.

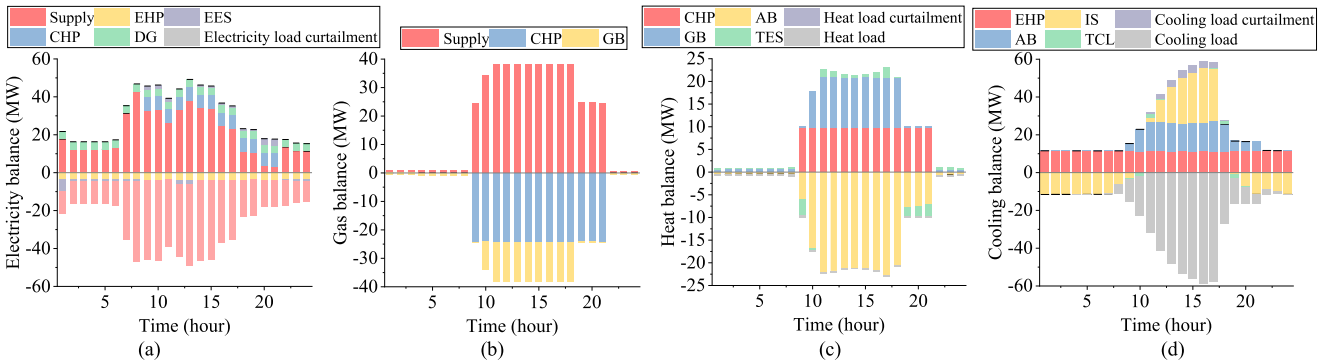

Fig. 8. Energy balance of the UMES in S3: (a) Electricity balance; (b) Gas balance; (c) Heat balance; (d) Cooling balance.

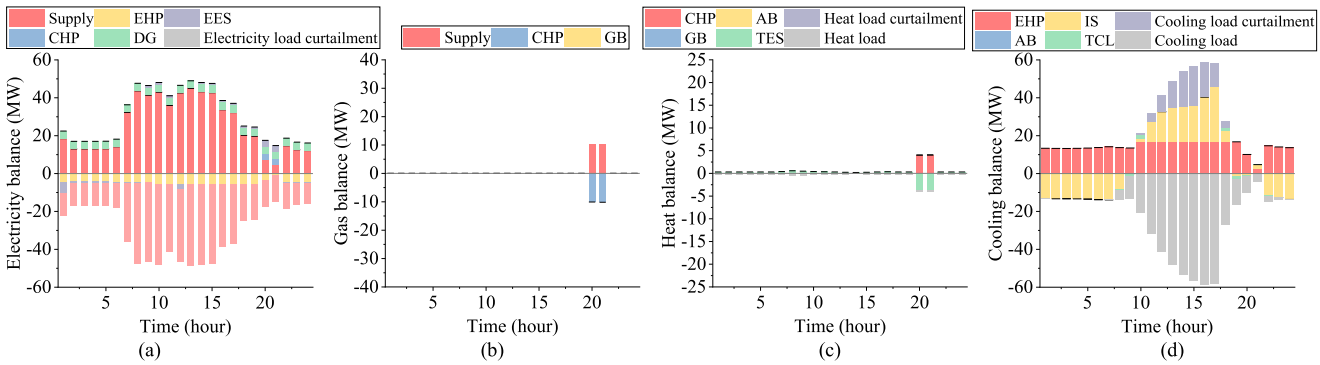

Fig. 9. Energy balance of the UMES in S6: (a) Electricity balance; (b) Gas balance; (c) Heat balance; (d) Cooling balance.

heat supply and demand are almost reduced to zero, as shown in Fig. 9(c) and (d), respectively.

To sum up, the UMES can well balance the energy supply and demand in most scenarios. When severe failure happens, load curtailment may occur, and CMS is required. Moreover, the UMES is highly dependent on energy storage to balance energy production and demand in different time periods, as well as to improve cost-efficiency. The degradation cost of energy storage is relatively small compared with other costs. The equivalent energy storage of TCL is active in the CMS. Although the volume is small, its comfort cost is also lower than other kinds of costs, which might be a good potential resource to improve the operational reliability of the system.

C. *Impacts of TCLs on the Operational Reliabilities*

In this case, based on the conclusions derived from the last case, we further study the impact of both the physical energy storage and the equivalent energy storage by TCL on the operational reliability of UMES. First, three scenarios S1, S2, and S3 are compared. S1 is the base scenario. In S2, the TCL is not regarded as the equivalent energy storage in the CMS. In S3, the

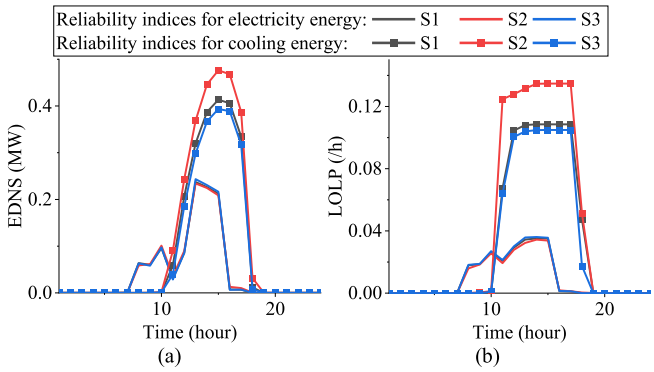

Fig. 10. Operational reliabilities of the UMES with different TCL settings: (a) EDNS; (b) LOLP.

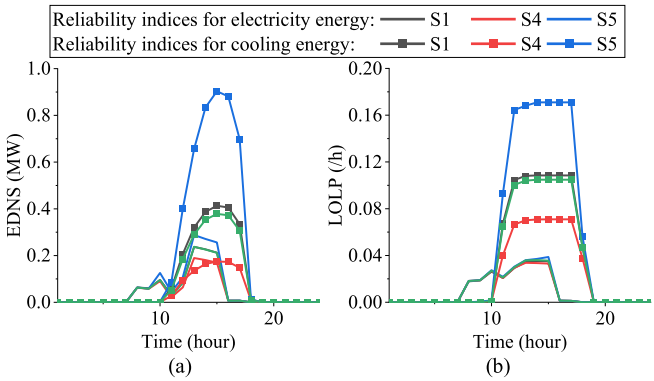

Fig. 11. Operational reliabilities of UMES with different energy storages: (a) EDNS; (b) LOLP.

comfort zone of the TCL is expanded to [22], [30]°C compared with the comfort zone [24], [28]°C in S1.

The operational reliabilities of UMES in three scenarios are presented in Fig. 10. It can be seen that the electricity reliability indices $EDNS^{el}$and $LOLP^{el}$ are close in the three scenarios. This indicates the participation of TCL in the CMS has little impact on electricity reliability. By comparing S1 and S2, the average EDNS and LOLP of the cooling energy increase by 17.49% and 28.05% in S2, respectively. By comparing S1 and S3, the average EDNS and LOLP of the cooling energy reduce by 6.55% and 7.39%, respectively. Therefore, TCL's participation in CMS improves the operational reliability of the UMES, though the volume of the TCL is small.

The effect of physical energy storage in improving operational reliability is validated by three scenarios from S4 $\sim$ S6. In S4, an IS with identical physical parameters is added to the UMES. In S5, an IS is removed from the UMES. In S6, an IS that has the identical equivalent capacity as TCL (2.10 MW) is supplemented. The simulation results are presented in Fig. 11. It can be seen that the increase in IS will significantly improve the operational reliability of both electricity and cooling energies. With an additional IS storage in S4, the average EDNS and LOLP of electricity reduce by 17.38% and 1.36%, respectively; the EDNS and LOLP of cooling energy reduce by 56.78% and 34.55%, respectively. With the removal of an IS in S5, the average EDNS and LOLP of the electricity increase by 19.61% and 5.09%, respectively; and the EDNS and LOLP of cooling energy increase by 109.15% and 53.19%, respectively.

S3 and S6 are compared to demonstrate the functions of the physical energy storage of IS and the equivalent energy storage of TCL. The increased capacity of the IS in S6 and equivalent energy storage in S3 are the same. However, the reliability in S6 is inferior to S3. The EDNS and LOLP of cooling energy in S6 are 2.44% and 4.31% larger than those in S3, because the TCL is a distributed resource with higher overall reliability. Thus, the reliability of UMES with TCLs is better than that with ISs in cases with the same increased capacity of energy storage.

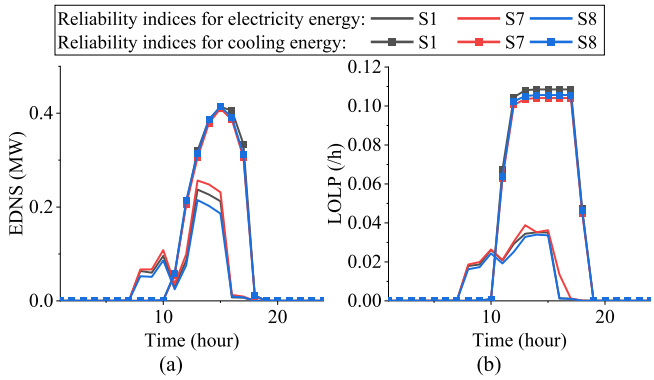

Fig. 12. Operational reliabilities of the UMES with different EES capacities: (a) EDNS; (b) LOLP.

D. Impacts of EESs on the Operational Reliabilities

The impact of EESs on the overall operational reliabilities of the UMES is studied in this section. First, we compare EESs with different capacities to show the impacts of EES sizing [55]. Two additional scenarios S7 and S8 are set to compare with the base scenario S1 in the last section. The capacities of each EES in S7 and S8 are set to 0.75 and 1.25 times of the original value, respectively.

The operational reliabilities of the UMES are presented in Fig. 12. We find that the operational reliabilities of electricity are significantly improved with the increase of EES capacity. From S2 to S1, and S1 to S3, the average EDNSs are reduced by 9.67% and 11.36%, respectively, and the LOLP is also reduced by 9.05% and 6.66%, respectively. This is because, with the increase of EES capacity, the UMES can use more electricity stored in the EES if the CHP or some of the EESs fail. The heat and cooling supplies do not tightly rely on the EES, and therefore the operational reliabilities of heat and cooling energies are almost the same in three scenarios. It means that the increase in the size of the EES is not that cost-efficient for improving the reliabilities of heat and cooling energies.

Second, to reflect the practical characteristics of the EES, we further set up three groups of comparative studies. In group 1, considering the nonlinear aging properties of the EES, the change in UMES's operational reliabilities caused by different EES conditions is compared. Two additional scenarios S9 and S10 are set to compare with S1. In S9, the EESs have never been

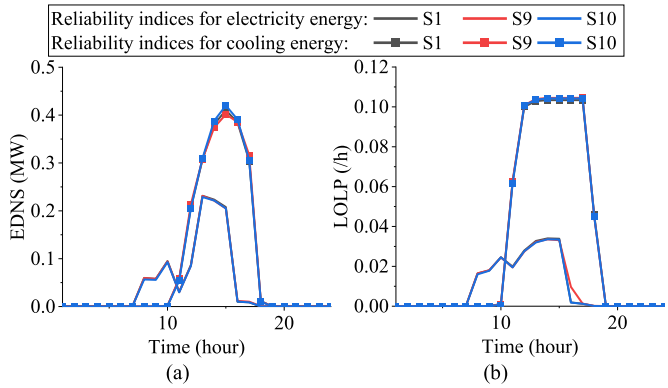

Fig. 13. Operational reliabilities of the UMES with different EES cycle times: (a) EDNS; (b) LOLP.

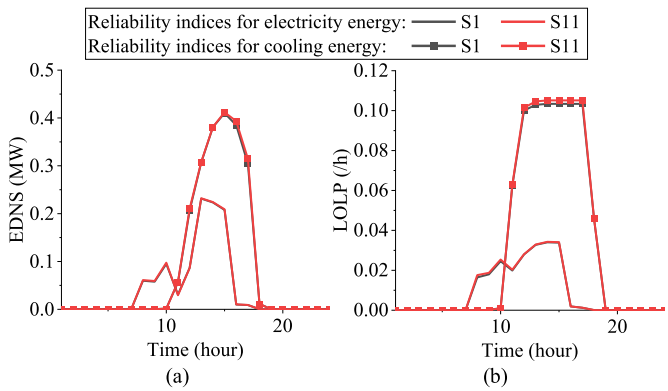

Fig. 14. Operational reliabilities of the UMES with/without considering the nonlinear charging/discharging power: (a) EDNS; (b) LOLP.

cycled before. In S10, the EESs have been cycled 40000 times. In group 2, we set scenario S11, which considers the nonlinear relations between charging/discharging power and the SOC. Its operational reliabilities are compared with S1. In group 3, the impacts of the response time of energy storages on operational reliabilities are investigated. Two scenarios S12 and S13 are set, where the response times of TESs and ISs are set to 0.5 and 1 hour, respectively.

The operational reliabilities of the UMES with different EES cycle times are presented in Fig. 13. We find that the cycle times have only a little impact on the operational reliabilities of the UMES. The EDNS of the electricity, and the LOLPs are almost the same. From scenarios S10 to S1, and from S1 to S9, the average EDNSs of the cooling energy decrease by 1.04% and 0.31%, respectively. This is because the cycle times affect the degradation cost in charging/discharging actions. Even in S10 where the degradation cost is high, it is still lower than the load curtailment cost. Therefore, the load curtailment is not affected, and the reliability indices in the three scenarios are almost the same.

The operational reliabilities of the UMES with/without considering the nonlinear charging/discharging power are presented in Fig. 14. We can find that the nonlinear charging/discharging power affects the cooling energy more than the electricity energy.

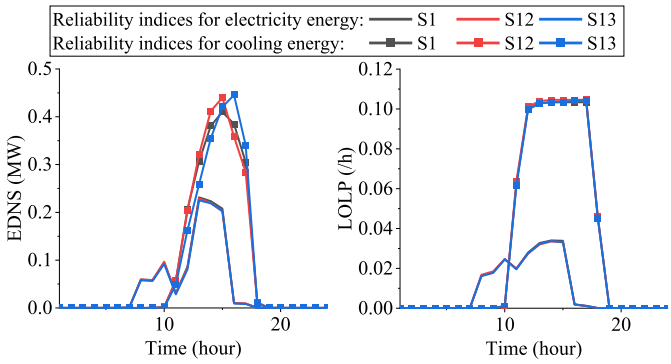

Fig. 15. Operational reliabilities of the UMES with different response times: (a) EDNS; (b) LOLP.

From S1 to S11, the reliability indices of the electricity are almost the same, while the EDNS and LOLP of the cooling energy increase by 1.23% and 1.45%, respectively. This is because by considering the nonlinear relationships, the discharging power of EES during the load peak hours decreases. The CHP needs to switch the operating mode to generate more electricity. Thus, the heat production is reduced, which affects the cooling production of AB. The reliability of cooling energy becomes inferior.

The operational reliabilities of the UMES with different response times are compared in Fig. 15. We find that the by considering the response time, the reliabilities of cooling energies become inferior. Compared with S1, the EDNSs of cooling energy in S12 and S13 increase by 1.18% and 1.15%, respectively. The LOLPs of cooling energy in S12 and S13 increase by 1.15% and 1.31%, respectively. Especially for EDNS, they increase in different patterns. This is because by considering the slower response time, the equivalent charging powers of IS and TES are reduced. In S12, the reduction of equivalent charging power is relatively slight, which mainly impacts 12:00-15:00 where the reliance on ISs is relatively small. While in S13, the reduction of equivalent charging power is more severe. It mainly impacts 16:00-17:00, during which the UMES heavily relies on the IS to provide cooling energy.

VII. Conclusion

This paper proposes an operational reliability evaluation framework of UMES, considering the flexibility provided by the equivalent energy storage from TCL. First, the concept of DEH is proposed as a unified tool to characterize the dynamic relationships between different components in the UMES. Then, the multi-state operational reliability of equivalent energy storage from the aggregated TCLs, as well as other key components in the UMES are modeled using the reliability equivalent technique. Moreover, the CMS of UMES is formulated, considering the degradation and comfort costs of different types of energy storage. Finally, an operational reliability evaluation procedure embedded with simplified Bender decomposition is developed.

By investigating typical contingency states, the numerical results validate the effectiveness of both physical and equivalent energy storages in minimizing load curtailment and

saving operating costs. From the operational reliability perspective, we find that though the volume of TCL is relatively small, it has good performance in improving the operational reliability of UMES.

The DEH model proposed in this paper describes the physical characteristics of UMES within the control theory framework. Thus, it lays a foundation for observability and controllability analysis in the future. The models, technical framework, and quantitative results in this paper can be used to assist the system operator in the day-ahead schedule, reliability management, economic or risk-based optimal control, etc., in the UMES. The combination of dynamics of thermal rating in the transmission lines and energy storages can exhibit better performance in the operational reliability. Therefore, future works can be further carried out considering the network topology by incorporating dynamics of thermal rating, gas flow, heat flow, energy storages, etc., into the reliability evaluation of UMES.

APPENDIX

A. Specific Form of the Dynamic Energy Hub Model

The specific elements of the DEH model are elaborated as follows. The energy flows between the node i and gas, electricity, heat, and cooling buses are denoted as f_i^g, f_i^e, f_i^h, and f_i^c, respectively. It should be noted that there is more than one choice for state variables, control variables, and output variables. Here we choose the capacity of EES, TES, IS, and TCLs as the state variables $\mathbf{x} = [es_8, es_9, es_{10}, es_{11}, es_{12}]^T$, choose the energy flows in the DEH as the control variables $\mathbf{u} = [f_3^g, f_4^g, f_5^e, f_7^e, f_8^e, f_{13}^e, f_6^h, f_9^h, f_{14}^h, f_{10}^c, f_{15}^c]^T$, and choose the energy consumption of DEH as output variables $\mathbf{y} = [f_1^g, f_2^e]^T$. The (2) is governed by three sets of constraints: the energy conservation constraints for energy buses, the energy conversion relationships for devices, and the charging and discharging constraints for energy storages. Assuming the direction of energy flow into the energy bus as positive, the specific elements of coefficient matrixes can be obtained as follows: $\boldsymbol{\alpha} = 0$; elements in $\boldsymbol{\beta}$ are $\beta_{1,5} = \beta_{2,8} = \beta_{3,10} = -1$, $\beta_{4,1} = -\gamma\eta_3^h$, $\beta_{4,2} = -\gamma\eta_4$, $\beta_{4,3} = -\gamma COP_5^h$, $\beta_{4,7} = \beta_{4,8} = \beta_{4,9} = \gamma$, $\beta_{5,3} = -(1-\gamma)COP_5^c$, $\beta_{5,7} = (\gamma - 1)\eta_6$, and $\beta_{5,10} = \beta_{5,11} = 1 - \gamma$; $\boldsymbol{\chi} = 0$; elements in $\boldsymbol{\delta}$ are $\delta_{1,1} = -1$, $\delta_{1,2} = 1$, $\delta_{2,1} = \eta_3^e$, and $\delta_{2,3} = \delta_{2,4} = \delta_{2,5} = \delta_{2,6} = -1$; η_3^h and η_3^c are the heat production and electricity generation efficiencies of CHP, respectively; η_4 is the efficiency of GB; η_6 is the efficiency of AB; COP_5^c and COP_5^h are the coefficient of performance of EHP for cooling and heating modes, respectively.

B. Calculation of Cycle Depth for EES

Take the discharging process as an example, the increase in cycle depth of the EES j can be written as:

$$\Delta\delta_{j,k} = f_{8,j,k}^e \Delta t / es_{8,j}^{\max} \tag{43}$$

where Δt is the length of each time step.

The cycle life loss of the EES Φ_j is a function of cycle depth δ_j, which can be expressed as [45]:

$$\Phi_j = \left(5.24 \times 10^{-4}\right) \delta_j^{2.03} \tag{44}$$

C. Quadratic Fitting of PPD Function

The PDD function in its original form can be written as [46]:

$$PPD(T) = 100 - 95e^{-\left(0.03353PMV^4(T) + 0.2179PMV^2(T)\right)} \tag{45}$$

where PMV is the Predicted Mean Vote index, which can be calculated as:

$$\begin{aligned} &PMV(T) \\ &= (0.303e^{-0.036M} + 0.028)\{M - W \\ &\quad - 3.05 \times 10^{-3} \times (5733 - 6.99(M - W) - P^a) \\ &\quad - 0.42\left((M - W) - 58.15\right) - 1.7 \times 10^{-5} M \\ &\quad (5867 - P^a) - 0.0014M \times (34 - T) - 3.96 \times 10^{-8} f^{cl} \\ &\quad \left(t^{cl} + 273\right)^4 - (t^r + 273)^4 - f^{cl} h^c (t^{cl} - T)\} \end{aligned} \tag{46}$$

where M is the metabolic rate; W is mechanical work; P^a is water vapor pressure; t^{cl} is the clothing temperature; t^r is mean radiant temperature; f^{cl} is the area coefficient of clothing; h^c is the convective heat transfer coefficient.

Then, the PPD can be fitted as a quadratic function as [47]:

$$PPD(T) = 0.3222T^2 - 16.7544T + 217.8072 \tag{47}$$

where we assume the most comfortable temperature is 26 °C in summer.

REFERENCES

[1] UN Habitat, "The strategic plan 2020-2023," 2022. [Online]. Available: https://unhabitat.org/the-strategic-plan-2020-2023

[2] U.S. Department of Energy, "Combined heat and power and microgrid installation databases," 2022. [Online]. Available: https://doe.icfwebservices.com/index

[3] Lvliang Daily. Jinneng datuhe thermal power co., ltd. Made every effort to repair unit 2 (in chinese), 2020. [Online]. Available: https://www.guifan.cc/tutorial/22712.html

[4] M. Geidl, G. Koeppel, P. Favre-Perrod, and B. Klockl, G. Andersson, and K. Frohlich, "Energy hubs for the future," *IEEE Power Energy Mag.*, vol. 5, no. 1, pp. 24–30, Jan./Feb. 2007.

[5] N. Zhao, B. Wang, L. Bai, and F. Li, "Quantitative model of the electricity-shifting curve in an energy hub based on aggregated utility curve of multi-energy demands," *IEEE Trans. Smart Grid*, vol. 12, no. 2, pp. 1329–1345, Mar. 2021.

[6] Z. Zhang, C. Wang, H. Lv, F. Liu, H. Sheng, and M. Yang, "Day-ahead optimal dispatch for integrated energy system considering power-to-gas and dynamic pipeline networks," *IEEE Trans. Ind. Appl.*, vol. 57, no. 4, pp. 3317–3328, Jul./Aug. 2021.

[7] W. Alharbi and K. Bhattacharya, "Incentive design for flexibility provisions from residential energy hubs in smart grid," *IEEE Trans. Smart Grid*, vol. 12, no. 3, pp. 2113–2124, May 2021.

[8] J. Hu, X. Liu, M. Shahidehpour, and S. Xia, "Optimal operation of energy hubs with large-scale distributed energy resources for distribution network congestion management," *IEEE Trans. Sustain. Energy*, vol. 12, no. 3, pp. 1755–1765, Jul. 2021.

[9] B. Zeng and Y. Luo, "Potential of harnessing operational flexibility from public transport hubs to improve reliability and economic performance of urban multi-energy systems: A holistic assessment framework," *Appl. Energy*, vol. 322, Sep. 2022, Art. no. 119488.

[10] F. S. Gazijahani, J. Salehi, and M. Shafie-khah, "Benefiting from energy-hub flexibilities to reinforce distribution system resilience: A pre-and post-disaster management model," *IEEE Syst. J.*, vol. 16, no. 2, pp. 3381–3390, Jun. 2022.

[11] M. K. Metwaly and J. Teh, "Probabilistic peak demand matching by battery energy storage alongside dynamic thermal ratings and demand response for enhanced network reliability," *IEEE Access*, vol. 8, pp. 181547–181559, 2020.

[12] C.-M. Lai and J. Teh, "Network topology optimisation based on dynamic thermal rating and battery storage systems for improved wind penetration and reliability," *Appl. Energy*, vol. 305, 2022, Art. no. 117837.

[13] Y. Li et al., "Dense skip attention based deep learning for day-ahead electricity price forecasting," *IEEE Trans. Power Syst.*, early access, Oct. 27, 2022.

[14] Y. Ding, Y. Lin, and M. J. Zuo, "Multiperformance measure multistate systems: General definitions and concepts," *IEEE Trans. Rel.*, vol. 70, no. 1, pp. 2–12, Mar. 2021.

[15] Y. Ding, Y. Hu, Y. Lin, and Z. Zeng, "Reliability analysis of multiperformance multistate system considering performance conversion process," *IEEE Trans. Rel.*, vol. 71, no. 1, pp. 2–15, Mar. 2022.

[16] E. M. Larsen, Y. Ding, Y.-F. Li, and E. Zio, "Definitions of generalized multi-performance weighted multi-state K-out-of-n system and its reliability evaluations," *Rel. Eng. Syst. Saf.*, vol. 199, Jun. 2020, Art. no. 105876.

[17] S. Wang, C. Shao, Y. Ding, and J. Yan, "Operational reliability of multi-energy customers considering service-based self-scheduling," *Appl. Energy*, vol. 254, Nov. 2019, Art. no. 113531.

[18] C. Pan, Z. Bie, G. Li, C. Wang, and C. Yan, "Reliability evaluation of integrated energy system based on exergy," *CSEE J. Power Energy Syst.*, early access, Jan. 14, 2022.

[19] M. Z. Gargari and R. Ghaffarpour, "Reliability evaluation of multi-carrier energy system with different level of demands under various weather situation," *Energy*, vol. 196, Feb. 2020, Art. no. 117091.

[20] L. Chi et al., "Data-driven reliability assessment method of integrated energy systems based on probabilistic deep learning and Gaussian mixture model-hidden Markov model," *Renewable Energy*, vol. 174, pp. 952–970, May 2021.

[21] M. Cao et al., "Reliability tracing of the integrated energy system using the improved shapley value," *Energy*, vol. 260, Aug. 2022, Art. no. 124997.

[22] L. Chi et al., "A systematic framework for the assessment of the reliability of energy supply in integrated energy systems based on a quasi-steady-state model," *Energy*, vol. 263, Oct. 2022, Art. no. 125740.

[23] H. Ren, Z. Jiang, Q. Wu, Q. Li, and Y. Yang, "Integrated optimization of a regional integrated energy system with thermal energy storage considering both resilience and reliability," *Energy*, vol. 261, Sep. 2022, Art. no. 125333.

[24] Y. Ding, W. Cui, S. Zhang, H. Hui, Y. Qiu, and Y. Song, "Multi-state operating reserve model of aggregate thermostatically-controlled-loads for power system short-term reliability evaluation," *Appl. Energy*, vol. 241, pp. 46–58, Mar. 2019.

[25] M.-H. Shariatkhah, M.-R. Haghifam, M. Parsa-Moghaddam, and P. Siano, "Evaluating the reliability of multi-energy source buildings: A new analytical method for considering the dynamic behavior of thermal loads," *Energy Buildings*, vol. 126, pp. 477–484, Aug. 2016.

[26] H. Hui, Y. Ding, W. Liu, Y. Lin, and Y. Song, "Operating reserve evaluation of aggregated air conditioners," *Appl. Energy*, vol. 196, pp. 218–228, Jun. 2017.

[27] H. Hui et al., "A transactive energy framework for inverter-based HVAC loads in a real-time local electricity market considering distributed energy resources," *IEEE Trans. Ind. Inform.*, vol. 18, no. 12, pp. 8409–8421, Dec. 2022.

[28] P. Yazdkhasti, C. P. Diduch, and A. Elkhateb, "A methodology to forecast the control capacity and control payback of a population of thermostatically controlled appliances in a demand-side management," *IEEE Can. J. Elect. Comput. Eng.*, vol. 44, no. 2, pp. 136–142, Jan./Mar. 2021.

[29] Y. Wan, C. Long, R. Deng, G. Wen, X. Yu, and T. Huang, "Distributed event-based control for thermostatically controlled loads under hybrid cyber attacks," *IEEE Trans. Cybern.*, vol. 51, no. 11, pp. 5314–5327, Nov. 2021.

[30] X. Gong, E. Castillo-Guerra, J. L. Cardenas-Barrera, B. Cao, S. A. Saleh, and L. Chang, "Robust hierarchical control mechanism for aggregated thermostatically controlled loads," *IEEE Trans. Smart Grid*, vol. 12, no. 1, pp. 453–467, Jan. 2021.

[31] X. Zhuang, C. Ye, Y. Ding, H. Hui, and B. Zou, "Data-driven reserve allocation with frequency security constraint considering inverter air conditioners," *IEEE Access*, vol. 7, pp. 120014–120022, 2019.

[32] H. Hui, Y. Ding, Y. Song, and S. Rahman, "Modeling and control of flexible loads for frequency regulation services considering compensation of communication latency and detection error," *Appl. Energy*, vol. 250, pp. 161–174, May 2019.

[33] H. Hui, Y. Chen, S. Yang, H. Zhang, and T. Jiang, "Coordination control of distributed generators and load resources for frequency restoration in isolated urban microgrids," *Appl. Energy*, vol. 327, Dec. 2022, Art. no. 120116.

[34] M. Chertkov and V. Chernyak, "Ensemble of thermostatically controlled loads: Statistical physics approach," *Sci. Rep.*, vol. 7, no. 1, Aug. 2017, Art. no. 8673.

[35] Y. Wang, J. Cheng, N. Zhang, and C. Kang, "Automatic and linearized modeling of energy hub and its flexibility analysis," *Appl. Energy*, vol. 211, pp. 705–714, Feb. 2018.

[36] W. Huang et al., "Reliability and vulnerability assessment of multi-energy systems: An energy hub based method," *IEEE Trans. Power Syst.*, vol. 36, no. 5, pp. 3948–3959, Sep. 2021.

[37] T. Xia, W. Huang, X. Lu, N. Zhang, and C. Kang, "Planning district multiple energy systems considering year-round operation," *Energy*, vol. 213, Sep. 2020, Art. no. 118829.

[38] M. Geidl, G. Koeppel, P. Favre-Perrod, B. Klockl, G. Andersson, and K. Frohlich, "Energy hubs for the future," *IEEE Power Energy Mag.*, vol. 5, no. 1, pp. 24–30, Jan./Feb. 2007.

[39] W. Huang, X. Zhang, K. Li, N. Zhang, G. Strbac, and C. Kang, "Resilience oriented planning of urban multi-energy systems with generalized energy storage sources," *IEEE Trans. Power Syst.*, vol. 37, no. 4, pp. 2906–2918, Jul. 2022.

[40] Shengwang-ee/operational-reliability-evaluation-of-urban-multi-energy-systems-with-equivalent-energy-storage, 2022. [Online]. Available: https://github.com/ShengWang-EE/Operational-Reliability-Evaluation-of-Urban-Multi-Energy-Systems-With-Equivalent-Energy-Storage

[41] H. Jia, Y. Ding, Y. Song, C. Singh, and M. Li, "Operating reliability evaluation of power systems considering flexible reserve provider in demand side," *IEEE Trans. Smart Grid*, vol. 10, no. 3, pp. 3452–3464, May 2019.

[42] R. Billinton and P. Wang, "Reliability-network-equivalent approach to distribution-system-reliability evaluation," *IEE Proc. - Gener., Transmiss. Distrib.*, vol. 145, no. 2, pp. 149–153, Mar. 1998.

[43] M. R. Haghifam and M. Manbachi, "Reliability and availability modelling of combined heat and power (CHP) systems," *Int. J. Elect. Power Energy Syst.*, vol. 33, no. 3, pp. 385–393, Mar. 2011.

[44] I. G. Moghaddam, M. Saniei, and E. Mashhour, "A comprehensive model for self-scheduling an energy hub to supply cooling, heating and electrical demands of a building," *Energy*, vol. 94, pp. 157–170, Jan. 2016.

[45] J. Vetter et al., "Ageing mechanisms in lithium-ion batteries," *J. Power Sources*, vol. 147, no. 1, pp. 269–281, Sep. 2005.

[46] K. Fabbri, "The indices of feeling—Predicted mean vote PMV and percentage people dissatisfied PPD," in *Indoor Thermal Comfort Perception*. Berlin, Germany: Springer-Verlag, 2015, pp. 75–125.

[47] K. Ma, Y. Yu, B. Yang, and J. Yang, "Demand-side energy management considering price oscillations for residential building heating and ventilation systems," *IEEE Trans. Ind. Inform.*, vol. 15, no. 8, pp. 4742–4752, Aug. 2019.

[48] R. Billinton and W. Zhang, "Enhanced adequacy equivalent for composite power system reliability evaluation," *IEE Proc. - Gener., Transmiss. Distrib.*, vol. 143, no. 5, pp. 420–426, Aug. 1996.

[49] S. Moradi, R. Ghaffarpour, A. M. Ranjbar, and B. Mozaffari, "Optimal integrated sizing and planning of hubs with midsize/large CHP units considering reliability of supply," *Energy Convers. Manage.*, vol. 148, pp. 974–992, Sep. 2017.

[50] C. Grigg et al., "The IEEE reliability test system-1996. A report prepared by the reliability test system task force of the application of probability methods subcommittee," *IEEE Trans. Power Syst.*, vol. 14, no. 3, pp. 1010–1020, Aug. 1999.

[51] Y. Ding, L. Cheng, Y. Zhang, and Y. Xue, "Operational reliability evaluation of restructured power systems with wind power penetration utilizing reliability network equivalent and time-sequential simulation approaches," *IEEE J. Modern Power Syst. Clean Energy*, vol. 2, no. 4, pp. 329–340, Dec. 2014.

[52] P. Mancarella and G. Chicco, "Real-time demand response from energy shifting in distributed multi-generation," *IEEE Trans. Smart Grid*, vol. 4, no. 4, pp. 1928–1938, Dec. 2013.

[53] S. Wang, Y. Ding, M. Zheng, and C. Ye, "Operational reliability evaluation of distributed multi-energy systems considering optimal control of energy storages," in *Proc. IEEE/IAS Ind. Commercial Power Syst. Asia*, 2021, pp. 182–187.

[54] J. Lofberg, "YALMIP: A toolbox for modeling and optimization in MATLAB," in *Proc. IEEE Int. Conf. Robot. Automat.*, 2004, pp. 284–289.
[55] F. Mohamad, J. Teh, and C.-M. Lai, "Optimum allocation of battery energy storage systems for power grid enhanced with solar energy," *Energy*, vol. 223, May 2021, Art. no. 120105.

Sheng Wang (Member, IEEE) received the B. Eng. and Ph.D. degrees in electrical engineering from Zhejiang University, Hangzhou, China, in 2021 and 2016, respectively. He is currently a Postdoctoral Fellow with the State Key Laboratory of Internet of Things for Smart City, University of Macau, Macau, China. His research interests include optimization and reliability evaluation of integrated energy systems, and the low-carbon strategy for urban energy systems.

Hongxun Hui (Member, IEEE) received the B.E. and Ph.D. degrees in electrical engineering from Zhejiang University, Hangzhou, China, in 2015 and 2020, respectively. From 2018 to 2019, he was a Visiting Scholar with the Advanced Research Institute, Virginia Tech, Blacksburg, VA, USA and the CURENT Center, University of Tennessee, Knoxville, TN, USA. He is currently a Research Assistant Professor with the State Key Laboratory of Internet of Things for Smart City, University of Macau, Macao, China. His research interests include optimization and control of power system, demand response, and Internet of Things technologies for smart energy.

Yi Ding (Member, IEEE) received the bachelor's degree in electrical engineering from Shanghai Jiaotong University, Shanghai, China, in 2000, and the Ph.D. degree in electrical engineering from Nanyang Technological University, Singapore, in 2007. He is currently a Professor with the College of Electrical Engineering, Zhejiang University, Hangzhou, China. His research interests include power systems reliability and performance analysis incorporating renewable energy resources, and engineering systems reliability modeling and optimization.

Chengjin Ye (Member, IEEE) received the B.E. and Ph.D. degrees in electrical engineering from Zhejiang University, Hangzhou, China, in 2010 and 2015, respectively. From 2015 to 2017, he was a Distribution System Engineer with the Economics Institute, State Grid Zhejiang Electric Power Company Ltd. From 2017 to 2019, he was an Assistant Research Fellow with the College of Electrical Engineering, Zhejiang University where he has been a Tenure-track Professor since 2020. His research interests mainly include grid resilience enhancement, and market mechanism and control strategy towards the integration of demand resources into power system operation.

Menglian Zheng (Member, IEEE) received the bachelor's degree in energy and environmental systems engineering from Zhejiang University, Hangzhou, China, in 2011, and the Doctoral degree in earth and environmental engineering from Columbia University, New York, NY, USA, in 2015. She is currently an Associate Professor with the College of Energy Engineering, Zhejiang University. Her research interests include demand response, flow batteries, and smart grids.